



Fabrication and characterization of starch-*cl*-poly(lactic acid-*g*-acrylamide) nanohydrogel for adsorptive removal of Eriochrome Black-T from the aqueous medium

Inamuddin

Chemistry Department, Faculty of Science, King Abdulaziz University, Jeddah 21589, Saudi Arabia,
email: inamuddin@rediffmail.com (Inamuddin)

Received 25 February 2018; Accepted 2 May 2018

ABSTRACT

In this paper, starch-*cl*-poly(lactic acid-*g*-acrylamide) nanohydrogel(ST-*cl*-poly(LA-*g*-AAm) (NHG) was fabricated using co-graft/crosslinking polymerization method. Synthesized nanohydrogel has been characterized by Fourier-transform infrared spectroscopy (FTIR), transmission electron microscopy (TEM), and scanning electron microscopy (SEM). It has been found to be a proficient adsorbent for the elimination of highly noxious Eriochrome Black T (EBT) from aqueous solution. Effect of various parameters such as concentration of adsorbate, temperature, pH, contact time and adsorbent dosage was thoroughly studied. The highly acidic medium was found to be an operative medium for the maximum adsorption. Isotherm studies revealed that Langmuir model explained better adsorption process compared to those of Freundlich and Temkin indicating the monolayer adsorption of EBT onto ST-*cl*-poly(LA-*g*-AAm) NHG. Kinetic studies have shown that the adsorption can be better explained by pseudo- first-order kinetics.

Keywords: Nanohydrogel; Adsorption; Eriochrome Black-T; Grafting; Polymerization

1. Introduction

Hydrogels represent a class of soft-materials having 3-dimensional (3D) regular polymeric networks. They have high water binding and retaining capability. Depending upon the type of bonding between the 3D polymeric networks, hydrogels can be classified into two; chemical hydrogels and physical hydrogels. Physical hydrogels are mainly inter-linked through hydrogen bonds, coordination bonds or hydrophobic interactions, etc. [1,2]. Due to weak interactions, physical hydrogels readily respond to the external stimuli, such as pH, temperature or light, etc. and low mechanical strength deteriorates or limits their industrial and biomedical applications [3,4]. A number of approaches have been put forward for increasing their strength such as cross-linking with graphene, cellulose, carbon nanotubes, graphene oxide and clays, etc. Hydrogels have the tendency

to swell and their swelling ability is greatly affected by the pH, temperature, light irradiation, electric field, etc. [5–10]. Important factors determining the equilibrium swelling area degree of crosslinking, interaction with the counter ions and hydrophobic/hydrophilic interactions [11–13]. The hydrophilic nature of the hydrogels is due to the presence of active groups such as carboxylic (–COOH), hydroxylic (–OH), sulphonic (–SO₃H) and primary amidic (–CONH₂), etc. In spite of their high tendency towards water adsorption, they exhibit swelling behaviour instead of dissolving in the surrounding liquid [14–19]. Their high hydrophilicity, high swelling ratio, and biocompatibility increase their utility for different applications such as drug delivery, biosensors, and water purification, etc. [20–26].

Starch is a biopolymer and has great utility for a number of applications. It has been substituted for a number of traditionally used non-biodegradable or non-renewable materials and it acts as an efficient support for various compounds [27–32]. In addition to its biocompatible nature, other major positive aspects include its inexpensive nature, easy and abundant availability, etc. High mechanical and

*Corresponding author.

water retaining properties of starch can be improved to a great extent by co-grafting and crosslinking approach [33–37]. Due to its high positive aspects, it is used in different fields such as chemistry, biology, and biotechnology, etc.

Azo dyes constitute the major class of commercial dyes being used for various industrial applications due to their low cost and high versatility. One of the azo dyes, Eriochrome Black-T which is being utilized in various industries such as wool, nylon and silk as a dyeing agent. In addition, also used in laboratories as a complexometric agent for the determination of calcium, magnesium and zinc ions from aqueous solution. In spite of a number of uses, it is quite hazardous to the environment. It produces an intermediate product, naphthoquinone, one of the highly carcinogenic intermediates. So, its removal from the water bodies after use is a must. In the same context, the synthesis of starch-*cl*-poly(lactic acid-*g*-acrylamide) nanohydrogel using co-graft/crosslinking polymerization method was developed. Synthesized nanohydrogel was characterized by FTIR, TEM, and SEM. The adsorption ability of the nanohydrogel was utilized for the removal of toxic EBT from the aqueous solution. Different adsorption parameters such as temperature, pH, contact time, adsorbent dosage and concentration of dye were also been studied.

2. Experimental protocol

2.1. Reagents and instruments

Reagents used in the synthesis were lactic acid (CDHPvt. Ltd., India), acrylamide (LobaChemie), starch (LobaChemie), ammonium persulphate (APS) (CDH Pvt. Ltd., India), ammonium hydroxide (LobaChemie), sodium hydroxide (CDH Pvt. Ltd., India), *N,N'*-methylene-bis-acrylamide (LobaChemie). All solutions were prepared in double distilled water. Instruments used were an electronic balance, centrifuge machine, double beam UV spectrophotometer (INCO Instrument and Chemical Private Limited), Fouriertransform infrared spectrophotometer (Agilent Technologies Cary 630 FTIR), Scanning electron microscopy (JEOL Model, JSM 610) and Transmission electron microscopy (Techni G2 20 S-Twin).

2.2. Preparation of starch-*cl*-poly(lactic acid-*g*-acrylamide) nanohydrogel

The ST-*cl*-poly(LA-*g*-AAm)nanohydrogel was prepared by co-graft/crosslinking polymerization method. The first step involves graft polymerization of acrylamide onto lactic acid. For this 0.1 M solution of lactic acid and acrylamide were prepared in double distilled water and mixed in 1:1 (v/v) ratios. To the above mixture, 5% ammonium persulphate was added as initiator and the mixture was kept at 70°C for 2 h to obtain a lactic acid-grafted-acrylamide gel. In the second step, 3% starch solution was prepared in 50 mL double distilled water with constant stirring using a magnetic stirrer. To the above-prepared starch solution, the lactic acid-grafted-acrylamide gel was added dropwise in the presence of a crosslinker, *N,N'*-methylenebisacrylamide (MBAAm) (7%) w/w and initiator APS (5%) w/w. The reaction mixture was stirred for 3h at 70°C using a magnetic

stirrer. The ST-*cl*-poly(LA-*g*-AAm) nanohydrogel was collected using acetone and dried at 50°C in a hot air oven. The reaction yield was calculated using the formula:

$$\% \text{ Yield} = \frac{W_R - W_P}{W_R} \times 100 \quad (1)$$

where W_R is the weight of reactants and W_P is the weight of the product.

2.3. Characterization

FTIR spectrums for ST-*cl*-poly(LA-*g*-AAm) NHG before and after adsorption of EBT were recorded in the range of 400–4000 cm^{-1} by Fourier-transform infrared spectrophotometer using KBr disk method. A 20 mg of the ST-*cl*-poly(LA-*g*-AAm) nanohydrogel was mixed with 80 mg of KBr and then it was powdered. By applying a pressure of 80,000 psi, a transparent disk was molded. Microphotographs of nanohydrogels were recorded by using JEOL Model, JSM 610 scanning electron microscope (SEM). The two samples were placed on a carbon tape with silicone adhesive and mounted on an aluminium stub. The microphotographs were obtained at different magnifications. 3D structural representation of the synthesized nanohydrogel was determined by Techni G2 20 S-Twin transmission electron microscope (TEM). An electron beam was transmitted through a thin sample and was detected on the other side. This study helped in determining the particle size of the synthesized nanohydrogel. The net charge on the ST-*cl*-poly(LA-*g*-AAm) NHG was determined by pH_{pzc} using pH drift method.

2.4. Swelling behaviour of ST-*cl*-poly(LA-*g*-AAm) NHG

The swelling behaviour of ST-*cl*-poly(LA-*g*-AAm) NHG was evaluated in water. For this study, 500 mg of ST-*cl*-poly(LA-*g*-AAm) NHG was dissolved in water. After pre-defined time intervals, the ST-*cl*-poly(LA-*g*-AAm) NHG was removed from the water, pressed gently between the folds of filter paper and final weight of the nanohydrogel was noted. Percent swelling by the ST-*cl*-poly(LA-*g*-AAm) NHG was calculated using the formula [38]:

$$\% \text{ Swelling} = \frac{W_F - W_I}{W_I} \times 100 \quad (2)$$

where W_F represents the final weight of ST-*cl*-poly(LA-*g*-AAm) NHG after a pre-determined time interval and W_I represents the initial weight of ST-*cl*-poly(LA-*g*-AAm) NHG.

2.5 Adsorption of Eriochrome Black-T (EBT)

Adsorption of hazardous Eriochrome Black-T (EBT) dye from aqueous solution was examined by batch adsorption experiments. For carrying out the adsorption of EBT onto ST-*cl*-poly(LA-*g*-AAm) NHG parameters such as dye concentration, adsorbent dosage, pH, time and temperature were firstly optimized. After parameter optimization, the adsorption of dye was conducted in the set of 100 mL Erlenmeyer flasks, which were sealed and agitated at 200 rpm in an incubator shaker. Each Erlenmeyer flask was

filled with the optimized adsorbent amount and 50 mL of optimized EBT solution at 40°C. The pH of the EBT solution was adjusted with 0.1 N HNO₃/NaOH solutions. The experimental flasks were withdrawn at predetermined time intervals until the adsorption equilibrium was attained. The finally obtained dye solution was separated by centrifugation operated at 3500 rpm for 5 min. The supernatants were then filtered to ensure that solutions were free from ST-*cl*-poly(LA-*g*-AAM) NHG before measuring the remained out EBT concentration. The dye concentration in the solution at various time intervals was analyzed by double beam UV-visible spectrophotometer at 503 nm. Amount of dye adsorption per unit mass of ST-*cl*-poly(LA-*g*-AAM) NHG at equilibrium, q_e (mg g⁻¹) and % adsorption was evaluated using the following mass balance equations [39]:

$$q_e = \frac{(C_0 - C_e)}{m} \times V \quad (3)$$

$$\% \text{ Adsorption} = \frac{C_0 - C_e}{C_0} \times 100 \quad (4)$$

where C_0 and C_e are the initial and equilibrium concentration of EBT (mg L⁻¹), V is the volume of aqueous solution (L) and m is the amount of dry ST-*cl*-poly(LA-*g*-AAM) NHG (g).

The adsorption isotherm studies were carried out using 50 mL of 15ppm EBT solution and pH 3. With variation in the amount of adsorbent dose, the solution was subjected to thermostatic shaking with rpm 200 for 1 hour. Aliquots of the solution at pre-determined time interval were taken out and the data was utilized for evaluating various isotherms.

However, the kinetic studies were carried out at optimized EBT concentration of 15 ppm, adsorbent dosage of 20 mg and pH 3. The solution was then subjected to the thermostatic shaker at 200 rpm for 1 h. The sample was collected after every 10 min till 1 h and analyzed with the help of double beam UV-Visible spectrophotometer.

3. Result and discussions

3.1. Synthesis of starch-crosslinked-poly (lactic acid-grafted-acrylamide) nanohydrogel (ST-*cl*-poly(LA-*g*-AAM) NHG)

Starch-crosslinked-poly(lactic acid-grafted-acrylamide) nanohydrogel was fabricated by co-graft/crosslinking polymerization method [14]. Lactic acid was used as a comonomeric unit for the preparation of hydrogel due to its (a) high thermal stability (b) renewable, biocompatibility, energy saving nature and (c) non-toxic degradation products *i.e.* CO₂ and H₂O that are neither toxic nor carcinogenic to the human body. APS acts as an initiator that helped in initiating the reaction for formation of long polymeric chains and the N,N'-methylene bisacrylamide helped in cross-linking of these chains. Calculated % yield for the synthesized nanohydrogel is 82%. Fig. 1 shows the synthetic scheme for the preparation of ST-*cl*-poly(LA-*g*-AAM) NHG.

3.2. Swelling behaviour of ST-*cl*-poly(LA-*g*-AAM) NHG

The swelling behaviour of ST-*cl*-poly(LA-*g*-AAM) NHG is shown in Fig. 2. Results have shown that the swelling

behaviour mainly got affected due to the presence of functional groups such as -OH, -COOH, -NH and -CONH. Maximum swelling of 203% was observed for ST-*cl*-poly(LA-*g*-AAM) NHG after 7 h and after that percent swelling value remained constant.

3.3. Characterization

Fig. 3 shows the FTIR spectra of ST-*cl*-poly(LA-*g*-AAM) NHG before and after adsorption of EBT. In Fig. 3a broad peak at 1179 cm⁻¹ corresponds to the stretching of C-O group of the starch. Peaks at 1599 and 3235 cm⁻¹ are due to the C=O and O-H stretching vibrations of the starch, respectively [40–42]. Peak at 1390 cm⁻¹ is due to the -OH in-plane bending. The peak at 1479 cm⁻¹ is attributed to the occurrence of C-O stretching. C-H asymmetric stretching is confirmed by the peak at 2920 cm⁻¹. One absorption peaks corresponding to bending vibration of N-H is observed at 1568 cm⁻¹ [43–48]. Changes in the characteristic wavenumber of various bonds of ST-*cl*-poly(LA-*g*-AAM) in Fig. 2b confirm the adsorption of EBT onto ST-*cl*-poly(LA-*g*-AAM) NHG. The peak at 2995 cm⁻¹ is assigned to the aromatic -C-H stretching of mono-azo dye, EBT. The asymmetric stretching vibration of S-O in SO₃H has been confirmed by the appearance of a peak at 1198 cm⁻¹ and the symmetric stretching vibrations at 1054 cm⁻¹. N=N stretching vibration has been obtained at 1541 cm⁻¹. The characteristic peak of the NO₂ group has been observed at 1335 cm⁻¹. Figs. 4a,b show the SEM images of ST-*cl*-poly(LA-*g*-AAM) NHG at different magnifications. Both the images show the smooth surface of the synthesized nanohydrogel and the uniform distribution onto the starch moiety [49–52]. Fig. 5a,b show the TEM images of the synthesized nanohydrogel at different magnifications. Images confirmed the smooth and fibrous surface of the synthesized nanohydrogel. Fig. 6 shows the pH_{pzc} graph for the synthesized nanohydrogel. Observed value is 5.3 generalizing positive surface below this value and the negatively charged surface above 5.3.

3.4. Adsorption of EBT onto ST-*cl*-poly(LA-*g*-AAM) NHG

For undertaking the adsorption of EBT various parameters were optimized and discussed below:

3.4.1. Effect of dye concentration

The concentration of dye plays an important role in the adsorption process. Effect of concentration was studied at different concentrations in the range of 05–55 ppm as is depicted from Fig. 7a. Maximum adsorption of 64% is observed at 15 ppm which decreases to 22% with the increase of concentration to 55 ppm. The decrease in adsorption rate can be ascribed to the lesser availability of adsorbent sites due to increase in the concentration of adsorbate molecules.

3.4.2. Effect of contact time

Effect of contact time on the adsorption of EBT on nanohydrogel is shown in Fig. 7b. It is observed that with an

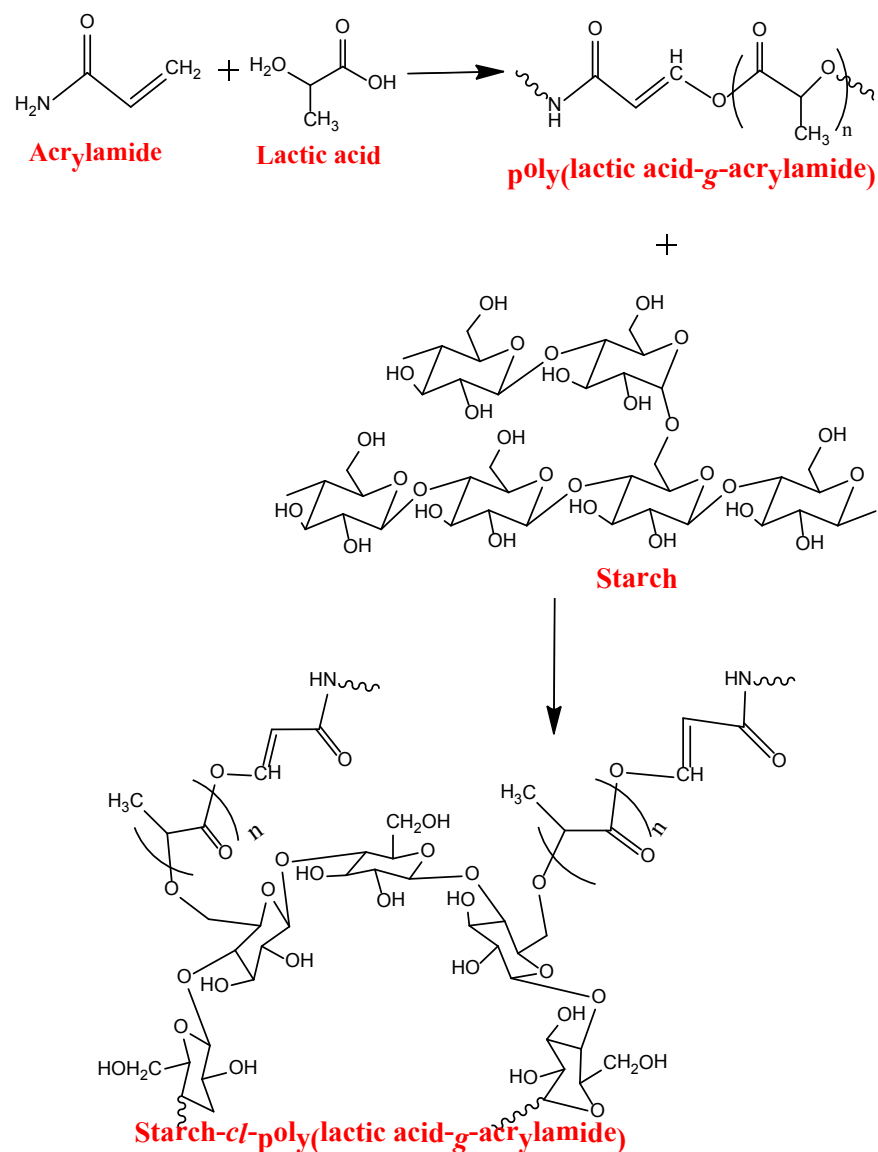


Fig. 1. Synthetic scheme for the formation of hydrogel.

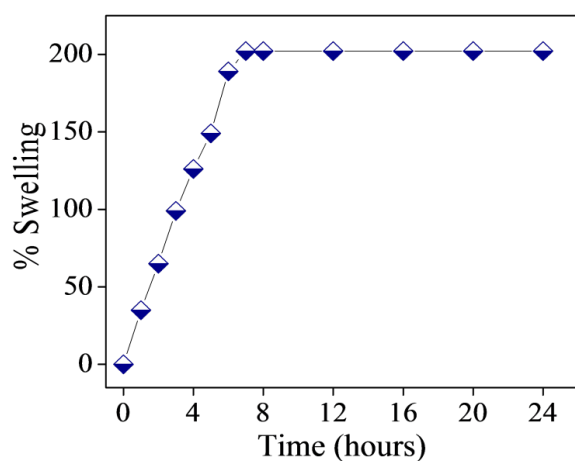


Fig. 2. Swelling behavior of ST-cl-poly(LA-g-AAm) NHG.

increase in contact time, the percent adsorption increases. Increase in contact time increases the probability of more interactions between the adsorbent and adsorbate molecules. Maximum of 79% adsorption is noted after 240 min and a further increase in time decreases the adsorption rate to only 33%. This decrease in the adsorption rate can be due to the lesser availability of adsorption sites.

3.4.3. Effect of pH

pH of the solution influences the rate of ionization of EBT molecules. The presence of highly reactive hydrogen or hydroxyl ions affects the adsorption rate to a large extent. The effect of pH on the adsorption of EBT on synthesized nanohydrogel was studied in the range of 1–9 (Fig. 7c). Results indicated that the adsorption of EBT is maximum in highly acidic medium and starts decreasing with the

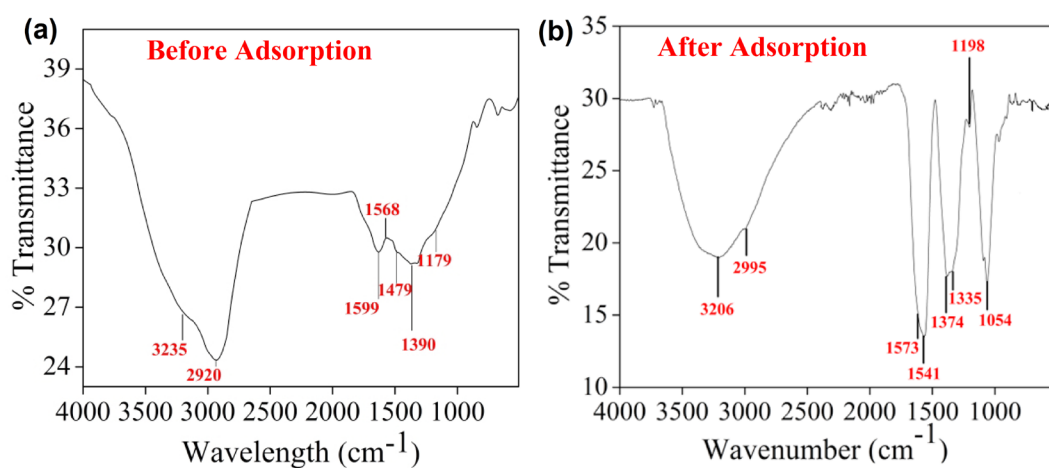


Fig. 3. FTIR spectrum of ST-cl-poly(LA-g-AAm) NHG (a) before adsorption and (b) after adsorption of Eriochrome Black-T.

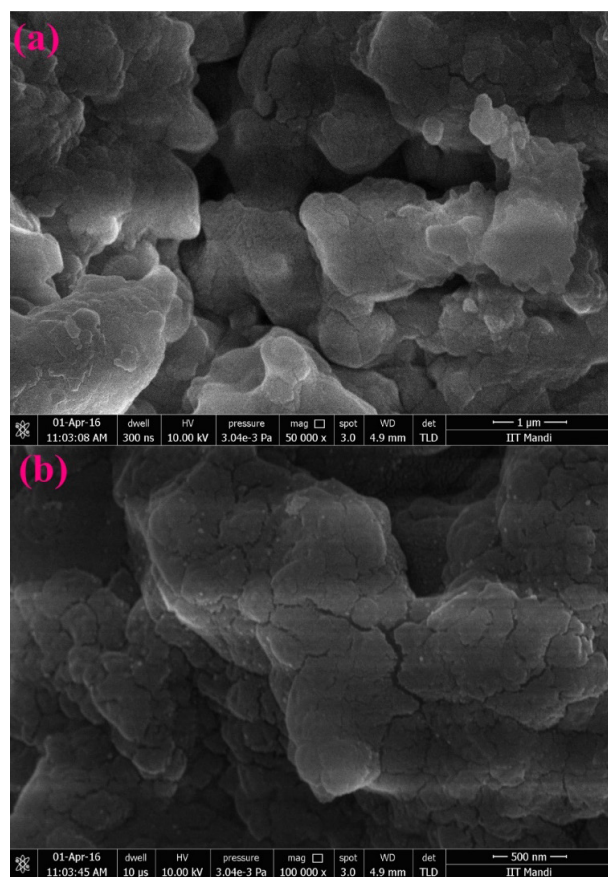


Fig. 4. SEM images of ST-cl-poly(LA-g-AAm) NHG.

rise in the pH value. pzc of ST-cl-poly(LA-g-AAm) NHG is 5.3 generalizing overall positively charged surface below 5.3. EBT is an anionic dye, so lower pH offers maximum interactions and thus, maximum adsorption. However, increase in pH increases the repulsive forces between the ST-cl-poly(LA-g-AAm) NHG and EBT molecules, as a result

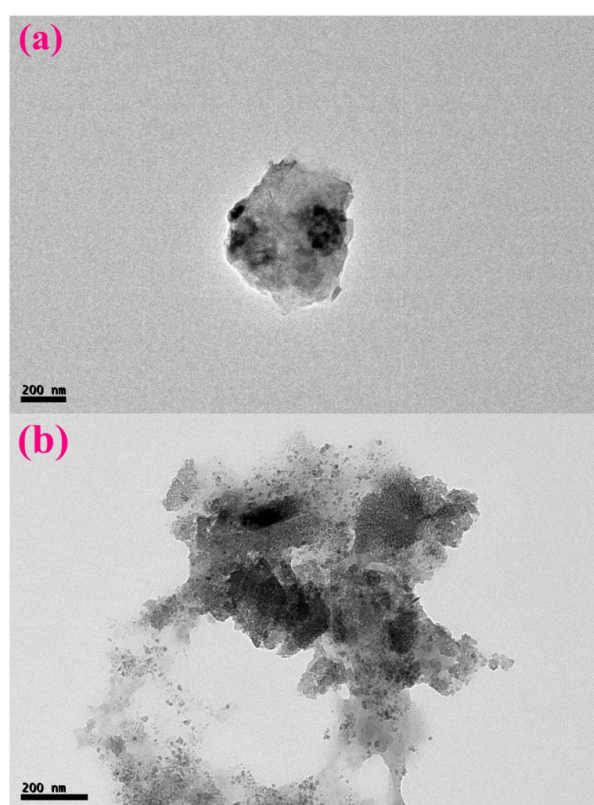


Fig. 5. TEM images of ST-cl-poly(LA-g-AAm) NHG.

of which % adsorption decreases. Maximum adsorption of 89% adsorption is noted at pH 3.

3.4.4. Effect of adsorbent dosage

Adsorbent dosage is an important adsorption parameter which helps in determining the overall ability of the adsorbent of adsorption for the optimized concentration of

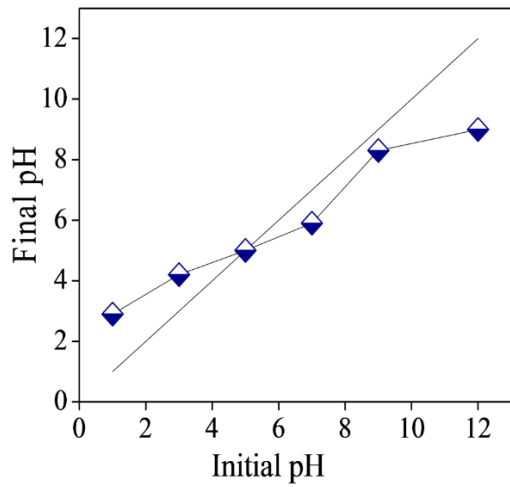


Fig. 6. pHpzc of ST-cl-poly(LA-g-AAm) NHG.

EBT. Effect of different adsorbent dosages was studied in the range of 5–30 mg. Percent adsorption increases from 23 to 74% with the increase in adsorbent dosage from 5 to 20 mg and then it starts decreasing. Increase in percent adsorption is probably due to increase in the binding sites and surface area of the adsorbent. However, when the adsorbent dosage exceeds a certain limit (20 mg), it resulted in a decrease of percent adsorption. Above 20 mg, the adsorbent molecules only increase the width of the layer and do not participate in further adsorption process [53,54].

3.4.5. Effect of temperature

Fig. 7e presents the effect of temperature on the rate of adsorption in the range of 20–70°C. Graphical trend represents that the rate first increases upto 60°C and then started decreasing generalizing the chemisorption of EBT onto ST-cl-poly(LA-g-AAm) NHG. High temperature generalizes the endothermic nature of the adsorption process.

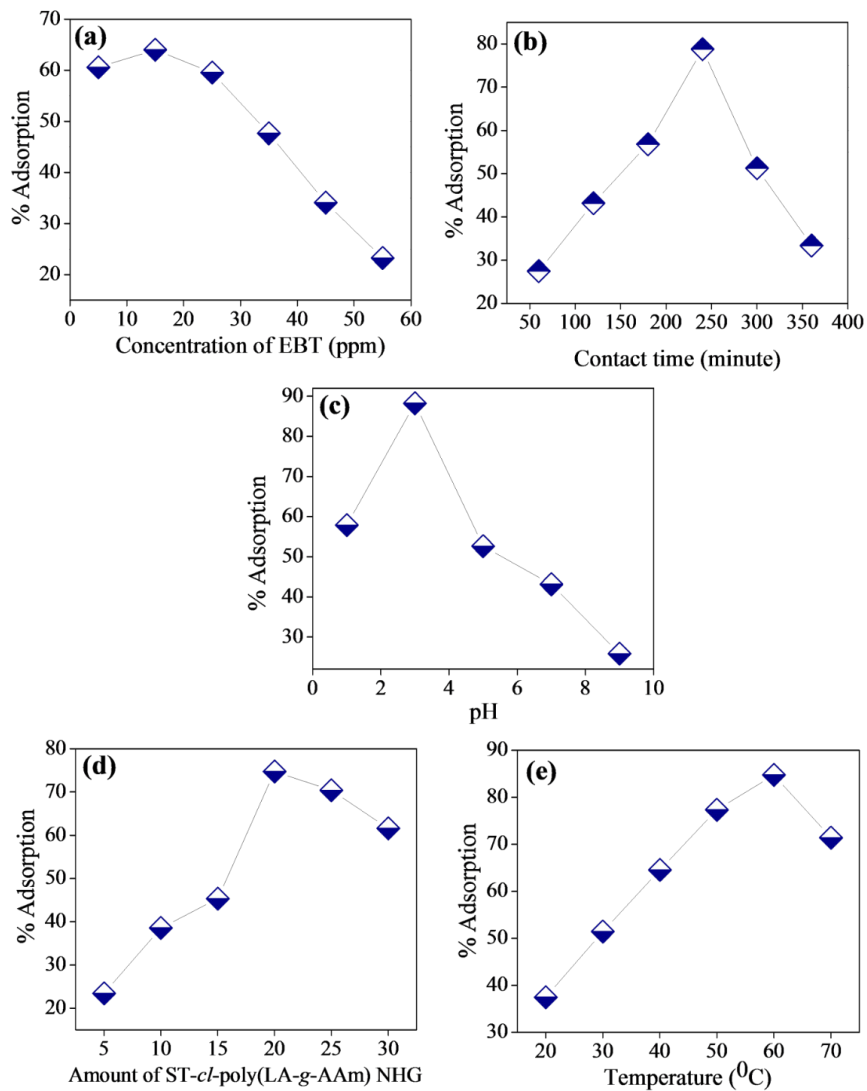


Fig. 7. Adsorption parameters (a) concentration of adsorbate (b) contact time (c) pH (d) adsorbate dosage (e) temperature.

3.5. Adsorption Isotherms

Isotherm studies helps in generalizing the type of adsorption process followed by the adsorbate molecules [55]. Different isotherm models studied are discussed below:

3.5.1. Langmuir isotherm

Langmuir isotherm generalize that the adsorbate molecules follows the monolayer adsorption on the adsorbent. It is given by the equation [20,56]:

$$\frac{C_e}{q_e} = \frac{C_e}{q_m} + \frac{1}{q_m K_L} \quad (5)$$

where q_e is the amount of EBT molecules adsorbed on the nanohydrogel (mg/g); C_e is the concentration of EBT adsorbed at equilibrium (mg/L); q_m and K_L are the Langmuir constants related to the adsorption capacity and adsorption energy, respectively [57]. The values of q_m and K_L were evaluated from slope and intercept of the adsorption isotherm when plotted between C_e and C_e/q_e [58]. Fig. 8a shows the Langmuir isotherm for the adsorption process. High correlation coefficient R^2 value of 0.966 has been obtained generalizing the monolayer adsorption of the EBT molecules on the ST-cl-poly(LA-g-AAm) NHG. The values of different rate constants are tabulated in Table 1.

3.5.2. Freundlich isotherm

Freundlich isotherm signifies the multilayer adsorption of adsorbate molecules on the energetically heterogeneous adsorbent surface sites. It can be clarified using the equation:

$$q_e = K_f C_e^{1/n} \quad (6)$$

where C_e (mg/L) is the concentration of EBT adsorbed at equilibrium; q_e (mg/g) is the amount of EBT adsorbed on nanohydrogel; K_f and n are the Freundlich constants related to the multilayer adsorption and adsorption intensity, respectively [59].

Table 1 shows different Freundlich constants for the adsorption process. R^2 value for this isotherm is 0.919 signifying the deviation of adsorption of EBT onto ST-cl-poly(LA-g-AAm) NHG from Freundlich isotherm.

3.5.3. Temkin isotherm

Temkin isotherm model assumes that heat of adsorption (which is a function of temperature) of all molecules in the layer would decrease linearly instead of logarithmic with coverage. This model is plotted between $\ln C_e$ and q_e and the constants were determined by the intercept and slope of the graph [60,61]. This model is given by the equation as follows:

$$q_e = B_i \ln K_T + B_i \ln C_e \quad (7)$$

where K_T is the Temkin isotherm equilibrium binding constant (L/g) and B_i constant related to the heat of sorption

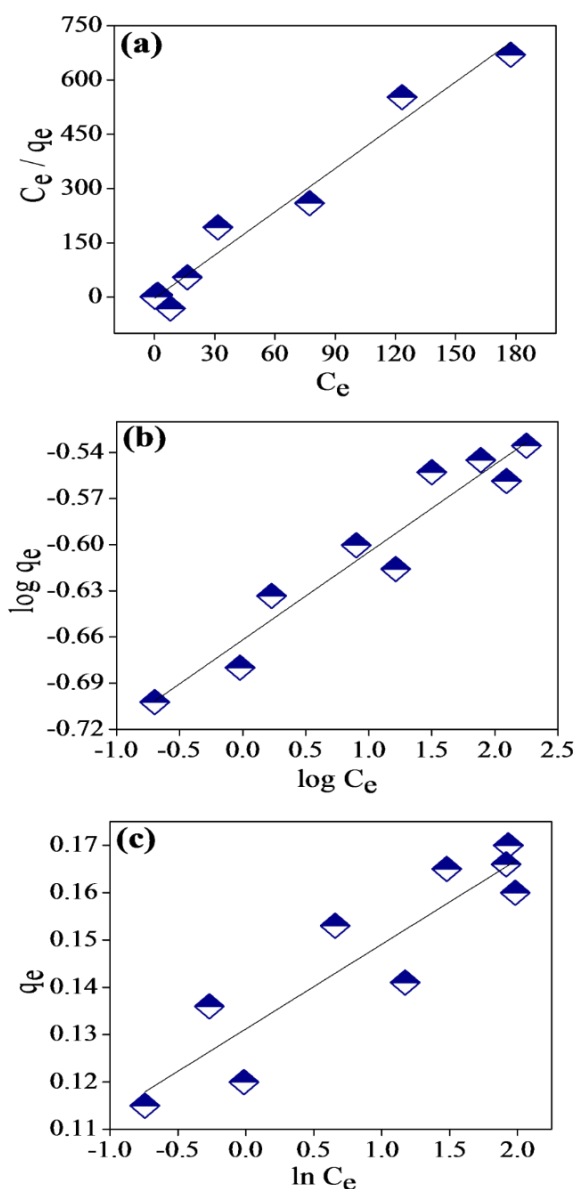


Fig. 8. Adsorption isotherms (a) Langmuir isotherm (b) Freundlich isotherm (c) Temkin isotherm.

(J/mol) [62,63]. Table 1 gives the values of different Temkin constants as calculated from the linear plots between $\ln C_e$ and q_e (Fig. 8c). Its lowest correlation coefficient value of 0.806 generalizes its maximum deviation from the adsorption process. Adsorption capacities of various adsorbents for EBT are presented in Table 2.

3.6. Adsorption kinetics

Kinetic studies of sorption process provide us important evidence such as the time required for attaining the equilibrium point, adsorption rate and prophecy of adsorbate concentration in each phase after the equilibrium is reached. Adsorption kinetics was carried out by studying pseudo

Table 1
Values of different constants for Langmuir, Freundlich and Temkin isotherm

S. No.	Model	Equation	Parameter	Value
1.	Langmuir	$\frac{C_e}{q_e} = \frac{C_e}{q_m} + \frac{1}{q_m K_L}$	q_m (mg/g)	56.834
			K_L (L/mg)	-0.006
			R^2	0.966
2.	Freundlich	$\log q_e = n \log C_e + \log K_F$	K_F (mg/g)	2.813
			n	-0.887
			R^2	0.919
3.	Temkin	$q_e = B_1 \ln K_T + B_1 \ln C_e$	(L/g)	0.134
			B_T	0.312
			R^2	0.806

Table 2
Adsorption capacities of various adsorbents for EBT

S. No.	Adsorbent	Maximum adsorption capacity (mg/g)	Reference
1.	Activated charcoal	4.71	[57]
2.	Titanate nanotubes	31	[58]
3.	Almond shell	6.02	[59]
4.	Cold plasma treated almond shell	18.18	[59]
5.	ST-cl-poly (LA-g-AAm) NHG	56.83	Present study

first order and pseudo-second-order kinetics [64]. Pseudo-first-order kinetics is based on the supposition that the mechanism following the adsorption is physical in nature. It also demonstrates that the adsorption occurs exclusively onto one site per ion [65]. It can better be explained by the following equation:

$$\log(q_e - q_t) = \log q_e - \frac{K_1}{2.303} \times t \tag{8}$$

where K_1 is the pseudo-first order rate constant. The values of the rate constants were determined from the slope of the plot between time (t) versus $\log(q_e - q_t)$. Pseudo-second order kinetics signifies the chemical interactions of adsorbate molecules with the adsorbent [66]. Pseudo-second order kinetics is given by the equation:

$$\frac{t}{q_t} = \frac{1}{k_2 q_e^2} + \frac{t}{q_e} \tag{9}$$

where k_2 is the overall rate constant for pseudo-second-order kinetics (g/mg/min); q_t is the quantity of EBT adsorbed at time t (mg/g) and q_e is the amount of EBT adsorbed at equilibrium (mg/g). Values of all constants of kinetic studies are compiled in Table 3. Higher correlation value for pseudo-first order as compared to pseudo-second-order kinetics generalizes the physical interactions between the adsorbate and adsorbent. Results are presented in Fig. 9.

Table 3
Values of different rate constants for pseudo first order, pseudo-second order and thermodynamics study

Pseudo-first order	K_1	q_e	R^2
	3.0035	0.332	0.98267
Pseudo-second order	K_2	q_e	R^2
	0.818	1.222	0.86193
Thermodynamics	ΔH^0	ΔS^0	ΔG^0
	15.33	47.48	-1.409

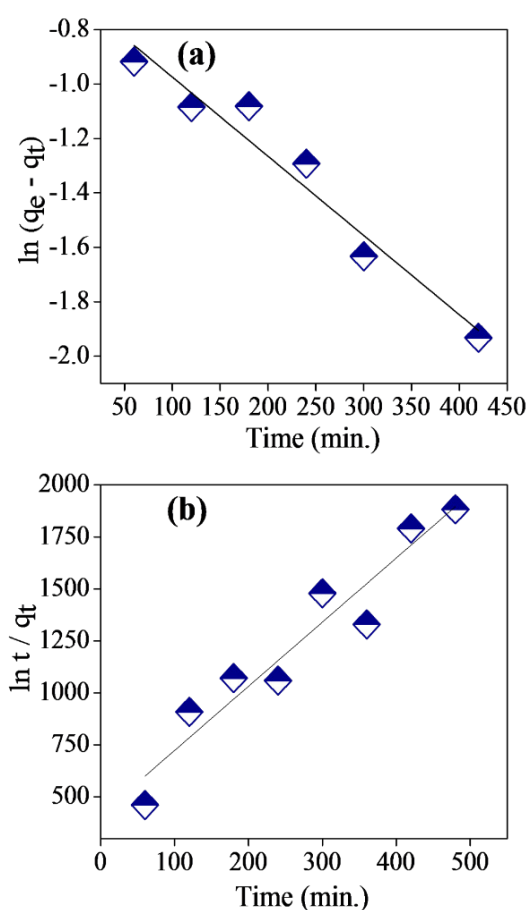


Fig. 9. Adsorption kinetics (a) Pseudo first order kinetics (b) Pseudo second order kinetics.

3.7. Thermodynamic Studies

Thermodynamic studies for the adsorption of EBT onto nanohydrogel has been carried out by studying the three factors *i.e.* ΔH^0 , ΔS^0 and ΔG^0 . The value of ΔG^0 at elevated temperatures can be calculated from the following equation [39]:

$$\Delta G^0 = \Delta H^0 - T\Delta S^0 \tag{10}$$

Values of ΔS^0 and ΔH^0 are calculated from the slope and intercept of the graph plotted between $1/T$ and $\ln q_e/$

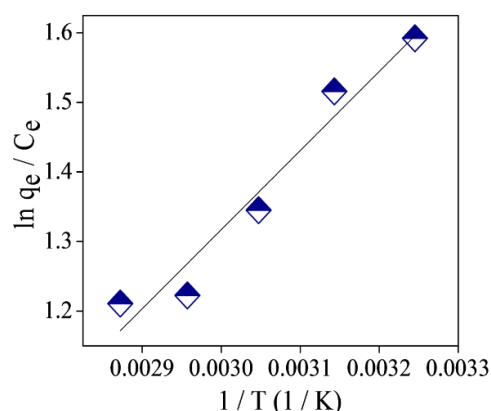


Fig. 10. Thermodynamics study for the adsorption process.

C_e (Fig.10). Thermodynamic studies help in elaborating the endothermic or exothermic nature of the adsorption process [14]. The calculated values of the three factors from Fig. 10 are presented in Table 3. The thermodynamic nature of the adsorption of EBT onto nanohydrogel can be examined from the changes of free Gibbs energy (ΔG^0), enthalpy (ΔH^0) and entropy (ΔS^0). The negative value of ΔG^0 (−1.409) signifies the spontaneous nature of the adsorption process and positive value of ΔH^0 (15.33) generalizes the endothermic nature of the adsorption process. Increase in randomness during the adsorption has been well explored by the positive value of ΔS^0 (47.48).

3.8. Desorption of adsorbed EBT

In order to regenerate the adsorbed ST-*cl*-poly(LA-*g*-AAm) NHG, the desorption studies were carried out to desorb the adsorbed EBT molecules from the surface of nanohydrogel. Studies on the pH effect showed that the adsorption was most probable in low pH or acidic medium generalizing that high pH or alkali solution may favour desorption. So, alkali solutions of NaOH and NH_4OH of various concentrations such as 0.05 M, 0.5 M, 1.0 M, 1.5 M and 2 M were used for evaluating the desorption efficiencies. Results presented in Fig. 11 show that the increase in the concentration of NaOH from 0.05 M to 2 M greatly enhanced the desorption rate from 38 to 89%. Enhancement in desorption rate from 22 to 67% was also been observed in case of NH_4OH but the result was more probable in case of NaOH determining strong alkali solutions of high concentration favouring the desorption of EBT from the surface of ST-*cl*-poly(LA-*g*-AAm) NHG.

3.9. Reusability

The reusability of ST-*cl*-poly(LA-*g*-AAm) NHG was determined for the adsorption of EBT molecules and the results are presented in Fig. 12. Percent adsorption decreased from 88 to 71% during the consecutive 6 cycles. The decrease in the adsorption ability of ST-*cl*-poly(LA-*g*-AAm) NHG with subsequent cycles can be due to the accumulation of EBT molecules onto the active sites leading to non-availability of sites for adsorption.

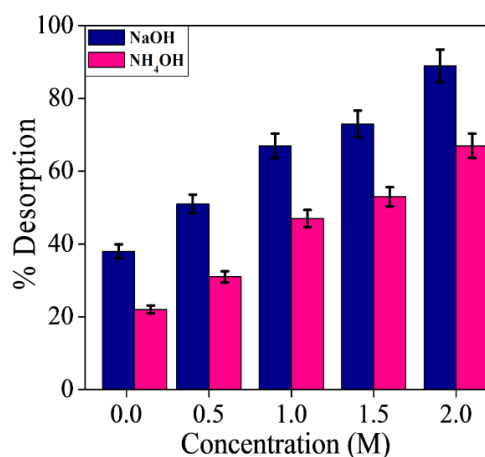


Fig. 11. Desorption studies of EBT from ST-*cl*-poly(LA-*g*-AAm) NHG surface by NaOH and NH_4OH .

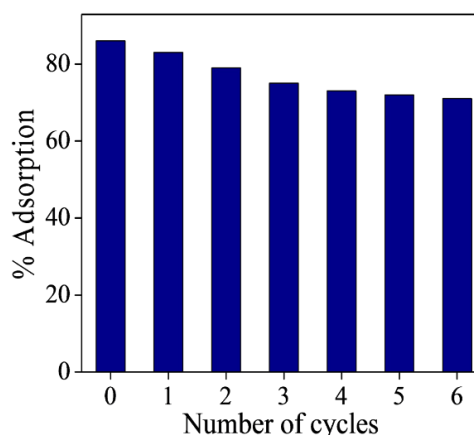


Fig. 12. Reusability studies of ST-*cl*-poly(LA-*g*-AAm) NHG.

4. Conclusion

Starch-*cl*-poly(lactic acid-*g*-acrylamide) nanohydrogel was prepared using co-graft/crosslinking polymerization method. The adsorption tendency of the synthesized nanohydrogel was studied for the adsorptional removal of noxious EBT dye from the aqueous solution. The prepared nanohydrogel was characterized by different techniques for the structural analysis. The adsorption of EBT on ST-*cl*-poly(LA-*g*-AAm) NHG followed pseudo-first-order kinetics and the equilibrium data fitted well with the Langmuir isotherm model. Thermodynamics studies showed the spontaneous nature of the adsorption process. A positive value of enthalpy change shows the endothermic nature of the adsorption process.

Acknowledgement

This work was supported by the Deanship of Scientific Research (DSR), King Abdulaziz University, Jeddah, under grant No. (D-149-130-1438). The author, therefore, gratefully acknowledge the DSR technical and financial support.

References

- [1] C. Chang, L. Zhang, Cellulose-based hydrogels : Present status and application prospects, *Carbohydr. Polym.*, 84 (2011) 40–53.
- [2] B. Raphael, T. Khalil, V.L. Workman, A. Smith, C.P. Brown, C. Streuli, A. Saiani, M. Domingos, 3D cell bioprinting of self-assembling peptide-based hydrogels, *Mater. Lett.*, 190 (2017) 103–106.
- [3] Q. Wang, S. Chen, D. Chen, Preparation and characterization of chitosan based injectable hydrogels enhanced by chitin, *J. Mech. Behav. Biomed. Mater.*, 65 (2017) 466–477.
- [4] G. Sharma, B. Thakur, M. Naushad, A. Kumar, Applications of nanocomposite hydrogels for biomedical engineering and environmental protection, *Environ. Chem. Lett.*, (2017) 1–34.
- [5] M. Rizwan, G.S.L. Peh, H. Ang, N. Chan, K. Adnan, J.S. Mehta, W. Siew, E.K.F. Yim, Biomaterials Sequentially-crosslinked bioactive hydrogels as nano-patterned substrates with customizable stiffness and degradation for corneal tissue engineering applications, *Biomaterials*, 120 (2017) 139–154.
- [6] S. Belali, A. Reza, M. Hadizadeh, Novel nanostructured smart, photodynamic hydrogels based on poly (N -isopropylacrylamide) bearing porphyrin units in their crosslink chains: A potential sensitizer system in cancer therapy, *Polymer*, 109 (2017) 93–105.
- [7] M. Rezakazemi, A. Vatani, T. Mohammadi, Synthesis and gas transport properties of crosslinked poly(dimethylsiloxane) nanocomposite membranes using octatrimethylsilyloxy POSS nanoparticles, *J. Nat. Gas Sci. Eng.*, 30 (2016) 10–18.
- [8] M. Rezakazemi, S. Shirazian, S.N. Ashrafizadeh, Simulation of ammonia removal from industrial wastewater streams by means of a hollow-fiber membrane contactor, *Desalination*, 285 (2012) 383–392.
- [9] M. Rezakazemi, M. Sadrzadeh, T. Mohammadi, T. Matsuura, Methods for the preparation of organic-inorganic nanocomposite polymer electrolyte membranes for fuel cells, 2017. doi:10.1007/978-3-319-52739-0_11.
- [10] M. Rezakazemi, M. Iravaninia, S. Shirazian, T. Mohammadi, Transient computational fluid dynamics modeling of pervaporation separation of aromatic/aliphatic hydrocarbon mixtures using polymer composite membrane, *Polym. Eng. Sci.*, 53 (2013) 1494–1501.
- [11] M. Rezakazemi, A. Dashti, M. Asghari, S. Shirazian, H₂-selective mixed matrix membranes modeling using ANFIS, PSO-ANFIS, GA-ANFIS, *Int. J. Hydrogen Energy*, 42 (2017) 15211–15225.
- [12] M. Rezakazemi, A. Ebadi Amooghin, M.M. Montazer-Rahmati, A.F. Ismail, T. Matsuura, State-of-the-art membrane based CO₂ separation using mixed matrix membranes (MMMs): An overview on current status and future directions, *Progress Polym. Sci.*, 39 (2014) 817–861.
- [13] E. Soroush, S. Shahsavari, M. Mesbah, M. Rezakazemi, Z. Zhang, A robust predictive tool for estimating CO₂ solubility in potassium based amino acid salt solutions, *Chinese J. Chem. Eng.* (2017). doi:10.1016/j.cjche.2017.10.002.
- [14] G. Sharma, M. Naushad, A. Kumar, S. Sharma, A. Bhatnagar, F.J. Stadler, Efficient removal of coomassie brilliant blue R-250 dye using starch/poly(alginic acid-*cl*-acrylamide) nanohydrogel, *Process Safety Environ. Protect.*, 109 (2017) 301–310.
- [15] S. Shirazian, M. Rezakazemi, A. Marjani, S. Moradi, Hydrodynamics and mass transfer simulation of wastewater treatment in membrane reactors, *Desalination*, 286 (2012) 290–295.
- [16] S. Shirazian, A. Marjani, M. Rezakazemi, Separation of CO₂ by single and mixed aqueous amine solvents in membrane contactors: Fluid flow and mass transfer modeling, *Eng. Comp.*, 28 (2012) 189–198.
- [17] M. Rezakazemi, A. Ghafarinazari, S. Shirazian, A. Khoshsima, Numerical modeling and optimization of wastewater treatment using porous polymeric membranes, *Polym. Eng. Sci.*, 53 (2013) 1272–1278. doi:10.1002/pen.23375.
- [18] M. Rezakazemi, A. Marjani, S. Shirazian, Development of a group contribution method based on UNIFAC groups for the estimation of vapor pressures of pure hydrocarbon compounds, *Chem. Eng. Technol.*, 36 (2013) 483–491.
- [19] M. Rostamizadeh, M. Rezakazemi, K. Shahidi, T. Mohammadi, Gas permeation through H₂-selective mixed matrix membranes: Experimental and neural network modeling, *Int. J. Hydrogen Energy*, 38 (2013) 1128–1135.
- [20] R. Foroutan, H. Esmaeili, M. Abbasi, M. Rezakazemi, M. Mesbah, Adsorption behavior of Cu(II) and Co(II) using chemically modified marine algae, *Environ. Technol.*, (UK). (2017) 1–9. doi:10.1080/09593330.2017.1365946.
- [21] M. Rezakazemi, Z. Niazi, M. Mirfendereski, S. Shirazian, T. Mohammadi, A. Pak, CFD simulation of natural gas sweetening in a gas-liquid hollow-fiber membrane contactor, *Chem. Eng. J.*, 168 (2011) 1217–1226.
- [22] M. Rezakazemi, M. Shahverdi, S. Shirazian, T. Mohammadi, A. Pak, CFD simulation of water removal from water/ethylene glycol mixtures by pervaporation, *Chem. Eng. J.*, 168 (2011) 60–67.
- [23] F. Hashemi, S. Rowshanzamir, M. Rezakazemi, CFD simulation of PEM fuel cell performance: Effect of straight and serpentine flow fields, *Math. Comp. Modelling*, 55 (2012) 1540–1557. doi:10.1016/j.mcm.2011.10.047.
- [24] A. Marjani, M. Rezakazemi, S. Shirazian, Vapor pressure prediction using group contribution method, *Oriental J. Chem.*, 27 (2011).
- [25] N. Azizi, M. Rezakazemi, M.M. Zarei, An intelligent approach to predict gas compressibility factor using neural network model, *Neural Comp. Appl.*, (2017). doi:10.1007/s00521-017-2979-7.
- [26] M. Mesbah, E. Soroush, Development of a least square support vector machine model for prediction of natural gas hydrate formation temperature, *Chinese J. Chem. Eng.*, 25 (2016) 26–32.
- [27] B. Liu, H. Xu, H. Zhao, W. Liu, L. Zhao, Y. Li, Preparation and characterization of intelligent starch/PVA films for simultaneous colorimetric indication and antimicrobial activity for food packaging applications, *Carbohydr. Polym.*, 157 (2017) 842–849.
- [28] X. Xiao, L. Yu, F. Xie, X. Bao, H. Liu, Z. Ji, L. Chen, One-step method to prepare starch-based superabsorbent polymer for slow release of fertilizer, *Chem. Eng. J.*, 309 (2017) 607–616.
- [29] S. Shirazian, M. Pishnamazi, M. Rezakazemi, A. Nouri, M. Jafari, S. Noroozi, A. Marjani, Implementation of the finite element method for simulation of mass transfer in membrane contactors, *Chem. Eng. Technol.*, 35 (2012) 1077–1084.
- [30] M. Fasihi, S. Shirazian, A. Marjani, M. Rezakazemi, Computational fluid dynamics simulation of transport phenomena in ceramic membranes for SO₂ separation, *Math. Comp. Model.*, 56 (2012) 278–286. doi:10.1016/j.mcm.2012.01.010.
- [31] M. Sadrzadeh, M. Rezakazemi, T. Mohammadi, Chapter 19 - Fundamentals and Measurement Techniques for Gas Transport in Polymers, in: S. Thomas, R. Wilson, A.K. S., S.C. George (Eds.), *Transport Properties of Polymeric Membranes*, Elsevier, 2018: pp. 391–423.
- [32] M. Rezakazemi, I. Heydari, Z. Zhang, Hybrid systems: Combining membrane and absorption technologies leads to more efficient acid gases (CO₂ and H₂S) removal from natural gas, *J. CO₂ Util.*, 18 (2017) 362–369.
- [33] E. Farno, M. Rezakazemi, T. Mohammadi, N. Kasiri, Ternary gas permeation through synthesized pdms membranes: Experimental and CFD simulation based on sorption-dependent system using neural network model, *Polym. Eng. Sci.*, 54 (2014) 215–226.
- [34] S.M.R. Razavi, M. Rezakazemi, A.B. Albadarin, S. Shirazian, Simulation of CO₂ absorption by solution of ammonium ionic liquid in hollow-fiber contactors, *Chem. Eng. Processing: Process Intensif.*, 108 (2016) 27–34.
- [35] A. Marjani, M. Rezakazemi, S. Shirazian, Simulation of methanol production process and determination of optimum conditions, *Oriental J. Chem.*, 28 (2012) 123–129.
- [36] M. Rezakazemi, S. Mirzaei, M. Asghari, J. Ivakpour, Aluminum oxide nanoparticles for highly efficient asphaltene separation from crude oil using ceramic membrane technology, *Oil Gas Sci. Technol.*, 72 (2017). doi:10.2516/ogst/2017031.

- [37] M. Rezakazemi, M. Sadrzadeh, T. Matsuura, Thermally stable polymers for advanced high-performance gas separation membranes, *Progr. Energy Combust. Sci.*, 66 (2018) 1–41.
- [38] P. Taylor, G. Sharma, M. Naushad, D. Pathania, A. Mittal, Treatment modification of Hibiscus cannabinus fiber by graft copolymerization: application for dye removal, *Desal. Water Treat.*, 54 (2014) 3114–3121.
- [39] M. Naushad, S. Vasudevan, G. Sharma, A. Kumar, Z.A. AlOthman, Adsorption kinetics, isotherms, and thermodynamic studies for Hg^{2+} adsorption from aqueous medium using alizarin red-S-loaded amberlite IRA-400 resin, *Desal. Water Treat.*, 57(39) (2016) 18551–18559.
- [40] V.K. Kotharangannagari, K. Krishnan, Biodegradable hybrid nanocomposites of starch/lysine and ZnO nanoparticles with shape memory properties, *Mater. Design*, 109 (2016) 590–595.
- [41] Z. Mahdiah, R. Bagheri, M. Eslami, M. Amiri, M.A. Shokrgozar, M. Mehrjoo, Thermoplastic starch/ethylene vinyl alcohol/forsterite nanocomposite as a candidate material for bone tissue engineering, *Mater. Sci. Eng. C.*, 69 (2016) 301–310.
- [42] M. Naushad, T. Ahamad, G. Sharma, A.H. Al-Muhtaseb, A.B. Albadarin, M.M. Alam, Z.A. AlOthman, S.M. Alshehri, A.A. Ghfar, Synthesis and characterization of a new starch/SnO₂ nanocomposite for efficient adsorption of toxic Hg^{2+} metal ion, *Chem. Eng. J.*, 300 (2016) 306–316.
- [43] D. Pathania, G. Sharma, A. Kumar, M. Naushad, S. Kalia, A. Sharma, Z.A. AlOthman, Combined sorptional – photocatalytic remediation of dyes by polyaniline Zr (IV) selenotungsto-phosphate nanocomposite, *Toxicol. Environ. Chem.*, 97 (2015) 526–537.
- [44] M. Rezakazemi, K. Shahidi, T. Mohammadi, Sorption properties of hydrogen-selective PDMS/zeolite 4A mixed matrix membrane, *Int. J. Hydrogen Energy*, 37 (2012) 17275–17284.
- [45] M. Rezakazemi, K. Shahidi, T. Mohammadi, Hydrogen separation and purification using crosslinkable PDMS/zeolite A nanoparticles mixed matrix membranes, *Int. J. Hydrogen Energy*, 37 (2012) 14576–14589.
- [46] M. Rezakazemi, T. Mohammadi, Gas sorption in H₂-selective mixed matrix membranes: Experimental and neural network modeling, *Int. J. Hydrogen Energy*, 38 (2013) 14035–14041.
- [47] M. Rezakazemi, A. Vatani, T. Mohammadi, Synergistic interactions between POSS and fumed silica and their effect on the properties of crosslinked PDMS nanocomposite membranes, *RSC Adv.*, 5 (2015) 82460–82470.
- [48] B. Baheri, M. Shahverdi, M. Rezakazemi, E. Motaeae, T. Mohammadi, Performance of PVA/NaA mixed matrix membrane for removal of water from ethylene glycol solutions by pervaporation, *Chem. Eng. Commun.*, 202 (2015) 316–321.
- [49] D. Pathania, G. Sharma, M. Naushad, V. Priya, A biopolymer-based hybrid cation exchanger pectin cerium(IV) iodate: synthesis, characterization, and analytical applications, *Desal. Water Treat.*, 57(1) (2016) 468–475.
- [50] G. Sharma, M. Naushad, A.H. Al-Muhtaseb, A. Kumar, M.R. Khan, S. Kalia, Shweta, M. Bala, A. Sharma, Fabrication and characterization of chitosan-crosslinked-poly(alginate) nanohydrogel for adsorptive removal of Cr(VI) metal ion from aqueous medium, *Int. J. Biol. Macromol.*, 95 (2017) 484–493.
- [51] M. Rezakazemi, K. Shahidi, T. Mohammadi, Synthetic PDMS composite membranes for pervaporation dehydration of ethanol, *Desal. Water Treat.*, 54 (2015) 1542–1549.
- [52] M. Rezakazemi, S. Razavi, T. Mohammadi, A.G. Nazari, Simulation and determination of optimum conditions of pervaporative dehydration of isopropanol process using synthesized PVA-APTEOS/TEOS nanocomposite membranes by means of expert systems, *J. Membr. Sci.*, 379 (2011) 224–232.
- [53] G. Sharma, A. Kumar, S. Sharma, M. Naushad, R. Prakash Dwivedi, Z.A. AlOthman, G.T. Mola, Novel development of nanoparticles to bimetallic nanoparticles and their composites: A review, *J. King Saud Univ. - Science.*, (2017). doi:10.1016/j.jksus.2017.06.012.
- [54] A. Mittal, M. Naushad, G. Sharma, Z. AlOthman, S. Wabaidur, M. Alam, Fabrication of MWCNTs/ThO₂ nanocomposite and its adsorption behavior for the removal of Pb (II) metal from aqueous medium, *Desal. Water Treat.*, 57 (2016) 21863–21869.
- [55] V.K. Gupta, G. Sharma, D. Pathania, N.C. Kothiyal, Nanocomposite pectin Zr(IV) selenotungsto phosphate for adsorption/photocatalytic remediation of methylene blue and malachite green dyes from aqueous system, *J. Ind. Eng. Chem.*, 21 (2015) 957–964.
- [56] M. Naushad, G. Sharma, A. Kumar, S. Sharma, A. Ghfar, A. Bhatnagar, F. Stadler, M. Khan, Efficient removal of toxic phosphate anions from aqueous environment using pectin based quaternary amino anion exchanger, *Int. J. Biol. Macromol.*, 106 (2018) 1–10.
- [57] D. Pathania, R. Katwal, G. Sharma, M. Naushad, M.R. Khan, A.H. Al-Muhtaseb, Novel guar gum/Al₂O₃ nanocomposite as an effective photocatalyst for the degradation of malachite green dye, *Int. J. Biol. Macromol.*, 87 (2016) 366–374.
- [58] M.I. Shariful, S. Bin Sharif, J.J.L. Lee, U. Habiba, B.C. Ang, M.A. Amalina, Adsorption of divalent heavy metal ion by mesoporous-high surface area chitosan/poly (ethylene oxide) nanofibrous membrane, *Carbohydr. Polym.*, 157 (2017) 57–64.
- [59] B.H. Hameed, F.B.M. Daud, Adsorption studies of basic dye on activated carbon derived from agricultural waste: Hevea brasiliensis seed coat, *Chem. Eng. J.*, 139 (2008) 48–55.
- [60] Y. Ho, Isotherms for the sorption of lead onto peat: comparison of linear and non-linear methods, *Polish J. Environ. Stud.*, 15 (2006) 81–86.
- [61] G. Sharma, M. Naushad, A. Kumar, S. Rana, S. Sharma, A. Bhatnagar, F.J. Stadler, A.A. Ghfar, M.R. Khan, Efficient removal of coomassie brilliant blue R-250 dye using starch/poly(alginate) nanohydrogel, *Process Safety Environ. Protect.*, 109 (2017) 301–310.
- [62] F. Wu, R. Tseng, High adsorption capacity NaOH-activated carbon for dye removal from aqueous solution, *J. Hazard. Mater.*, 152 (2008) 1256–1267.
- [63] F. Jamil, A.H. Al-muhtaseb, M. Naushad, M. Baawain, A. Al-mamun, S.K. Saxena, N. Viswanadham, Evaluation of synthesized green carbon catalyst from waste date pits for tertiary butylation of phenol, *Arabian J. Chem.*, (2017). doi:10.1016/j.arabjc.2017.04.009.
- [64] G. Sharma, A. Kumar, C. Chauhan, A. Okram, S. Sharma, D. Pathania, S. Kalia, Pectin-crosslinked-guar gum/SPION nanocomposite hydrogel for adsorption of m-cresol and o-chlorophenol, *Sustain. Chem. Pharm.*, 6 (2017) 96–106.
- [65] M. Rafatullah, O. Sulaiman, R. Hashim, A. Ahmad, Adsorption of copper (II), chromium (III), nickel (II) and lead (II) ions from aqueous solutions by meranti sawdust, *J. Hazard. Mater.*, 170 (2009) 969–977.
- [66] T. Wang, J. Liu, H. Huang, M. Fang, Z. Luo, Preparation and kinetics of a heterogeneous sorbent for CO₂ capture from the atmosphere, *Chem. Eng. J.*, 284 (2016) 679–686.